Quantum transport through cantori

N. T. Maitra[1,2,*] and E. J. Heller[1,2,3]
[1]*Department of Physics, Harvard University, Cambridge, Massachusetts 02138*
[2]*Harvard-Smithsonian Center for Astrophysics, Harvard University, Cambridge, Massachusetts 02138*
[3]*Department of Chemistry, Harvard University, Cambridge, Masschusetts 02138*
(Received 4 February 1999; revised manuscript received 2 December 1999)

We study the effect of classical cantori in quantum mechanics, extending previous results by several groups. We find that cantori form exponential barriers to quantum transport not only when Planck's constant exceeds the flux through the cantorus but also when it is smaller than the flux. The mechanism of localization in the two cases is different, and we describe the switch from dynamical localization to a mechanism we call ''retunneling'' as Planck's constant increases. We investigate the $\hbar$ dependence of the exponential decay for retunneling and find that the $\hbar^{-0.66}$ coefficient found previously at criticality appears to hold also away from criticality provided $\pi\hbar$ is large enough compared to the flux. Numerical evidence as well as an analytic argument are given. Our final contribution to this subject is a phase space view of cantori in quantum mechanics. We illustrate our results using the whisker map.

PACS number(s): 05.45.−a, 03.65.Sq

I. INTRODUCTION

The relation of the quantum mechanics of integrable systems to the underlying classical mechanics is well understood. Loosely speaking, one may think of the quantum mechanics as classical probability densities together with phases determined by classical actions and Maslov indices. In the integrable regime, EBK quantized energy states live on the invariant tori of classical phase space. (To paint the complete quantum picture and describe classically forbidden processes such as diffraction and tunneling, extension into complex coordinates must be made.)

Most systems however are not integrable. The quantum mechanics of systems with a chaotic component is not so well understood, although tremendous progress has been made in the last 30 years. Much insight has been gained into the statistical properties (e.g., eigenvalue spacing and eigenvector distributions) of the quantum mechanics of fully chaotic systems [1,2]. Indeed, semiclassical rules hold solidly for the quantization of such systems: the sum may be over a huge number of paths but is accurate as long as action differences between contributions are appreciable. This is often the case [3]. Near-integrable systems, with their mixed phase space, are less understood, yet of fundamental importance since typical atomic and molecular systems fall into this class. One can gain some understanding of the quantum behavior of such systems by considering the various structures generic to mixed phase space. States in surviving islets of stability surrounding stable periodic orbits or attached to invariant tori are quantized as in regular systems: such states lie on tori whose actions satisfy EBK quantization rules. The phase space area occupied by an islet must be at least Planck's constant, $h/2$, in order to be resolved by quantum mechanics. A quantum wave packet initially lying well within the islets can only tunnel to get out, with tunneling probability depending on Planck's constant as $e^{-S/\hbar}$ where S is an appropriate action.

Quantum states in the chaotic regions are generally quasiergodically distributed in the region (however, see Ref. [4] for scarred states), but localization of quantum states may occur when the classical diffusion time scale is larger than the quantization time (the time to resolve discrete levels in a phase space volume explored by the diffusion). In this case quantum transport across the chaotic region is also exponentially suppressed but with dramatically different characteristics, in particular a different $\hbar$ dependence, of the form $e^{-(\cdots)\hbar}$.

The structure that interests us in this paper in a sense falls in between integrable and chaotic: cantori, which are the remnants of an irrational winding number torus (KAM surface) at values of the nonlinearity parameter above but close to the critical value for break up. How these structures delay the classical transport in phase space has been thoroughly studied in pioneering work [5–7]. Remarkable results on the scaling properties and renormalization group theory near a cantorus at criticality are now well established [8,9].

In this paper we extend prior investigations [10–14] of the manifestations of cantori in quantum mechanics. The earlier studies have included elegant results on the exponential barriers that cantori present to quantum transport [11,13,14] and on how scaling carries over to quantum mechanics [10,15]. We extend this work in a number of ways. The earlier work had shown that cantori act as stronger (exponential) barriers to transport in quantum mechanics than in classical mechanics when $\hbar$ is big enough that quantum mechanics ''sees'' a closed surface rather than a broken one. However, we show there is also exponential localization for smaller $\hbar$ through a different mechanism, a dynamical localization effect. We demonstrate the crossover from dynamical localization to tunneling through a ''quantum-mechanically closed'' cantorus as $\hbar$ increases. Only at criticality, when the cantorus is just about to break up, are the characteristics of the transport quantified in the literature: the $\hbar$ dependence is

*Present address: Department of Chemistry, University of California at Berkeley, Berkeley, CA 94720-1460.

found to be $e^{-(\cdots)/\hbar^{0.66}}$. We find in this paper that this holds away from criticality as well, provided h is big enough compared to the classical flux crossing the cantorus. We provide numerical arguments as well as an analytic one for this behavior. We show how considering the evolution of states in the time domain can solidify our understanding about transport through cantori as can Husimi plots in phase space.

In Sec. II we briefly discuss some properties of cantori in classical mechanics. We illustrate them using a whisker map. We point out that our results hold for generic cantori in any map due to the universality of the dynamics near a cantorus. Section III explores the quantum dynamics near such cantori, discussing in detail the points raised in the previous paragraph.

The whisker map describes the motion around a separatrix in a typical (nonintegrable) system [16–18]. The separatrix is a ubiquitous structure in the phase space of generic nonlinear systems. A first-order analysis of a typical two-dimensional near-integrable system near a resonance yields a pendulum Hamiltonian in a pair of ''slow'' coordinate-momentum variables, with the ''fast'' action being an adiabatic invariant. A closer look reveals a chaotic layer around the slow variable's pendulum separatrix and a corresponding layer around the fast adiabatically constant action. Typically there is a thin layer of chaos around the separatrix, even for the smallest perturbation. As the perturbation increases, this layer grows to fill phase space.

The whisker map has the form

$$I' = I - k \sin\theta$$

$$\theta' = \theta + \lambda \ln\left|\frac{c}{I' - I_o}\right| \pmod{2\pi}. \tag{1}$$

This is a mapping in the ''fast'' variables I, θ. The parameter λ controls where the structures lie in phase space (islands, cantori); properties such as their size and stochasticity depend on both λ and k. The map has an infinite number of fixed points

$$I_r = I_o \pm c e^{-2\pi r/\lambda}, \quad \theta_r = 0 \text{ or } \pi, \tag{2}$$

where r is an integer. All fixed points with $|I_r - I_o| < \lambda k/4$ are unstable. The infinite number of unstable fixed points in this action range accumulate exponentially to I_o, their unstable manifolds overlapping. The fixed points ($\theta_r = 0, I_r > I_o + \lambda k/4$) and ($\theta_r = \pi, I_r < I_o - \lambda k/4$) are also unstable. Stable elliptic fixed points exist at ($\theta_r = \pi, I_r > I_o + \lambda k/4$) and ($\theta_r = 0, I_r < I_o - \lambda k/4$).

An example of the classical whisker map phase space is given in Fig. 1 where we have chosen parameter values $k = 2, \lambda = 5$, seeded 50 random initial conditions, and iterated the map 400 times. The points were plotted at each iteration. The motion appears chaotic for roughly $|I_r - I_o| < 10$, except in the islets. The width of the chaotic layer can be understood from transforming the behavior around the first-order resonances to local standard mappings. Expanding the logarithmic shearing term around the fixed point action, we find that the whisker map is locally

$$P' = P + k_{\text{eff}} \sin\theta,$$

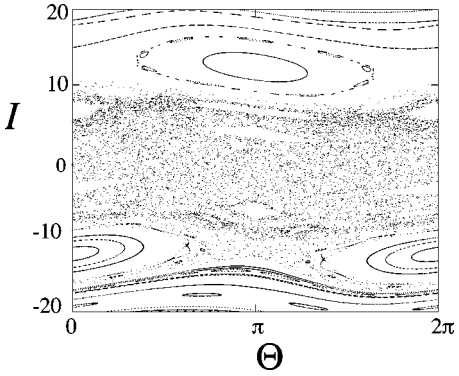

FIG. 1. Classical whisker map phase space: $\lambda = 5, k = 2$, with $I_0 = 0$ (see text).

$$\theta' = \theta + P'. \tag{3}$$

This is a standard map in the variables

$$\left(P = -\frac{\lambda}{I_r - I_o}(I - I_o), \theta \right) \tag{4}$$

with effective nonlinearity parameter

$$k_s = k_{\text{eff}} = \frac{\lambda k}{I_r - I_o}. \tag{5}$$

A standard map with $|k_s| > k_c = 0.9716354\cdots$ is globally chaotic (see the next section): a trajectory started in one area of phase space eventually travels over almost all of it, excluding only isolated islets of stability which shrink as $|k_s|$ grows. This implies that the half width I_c of the chaotic layer in the whisker map is

$$I_c \approx \lambda k / k_c. \tag{6}$$

The degree of stochasticity grows as the action moves deeper into the stochastic layer: k_{eff} increases from critical (k_c) at the layer's border to infinity in the middle at I_o. As a consequence, deep inside the chaotic layer the motion is very random and leads to diffusion in the action (Sec. II). Further out, the phase space has more structure: in addition to the islets of stability, there are cantori, remnants of KAM invariant tori which slow down the diffusion. There may be several cantori in various stages of disintegration within the layer, increasing in their transport inhibition as the border with the regular region is approached.

II. CANTORI IN CLASSICAL MECHANICS

Deep inside the stochastic layer the whisker map suffers diffusion in action:

$$\langle I(t) \rangle = \langle I(0) \rangle,$$
$$\langle I(t)^2 \rangle = \langle I(0)^2 \rangle + Dt, \quad D = k^2/2, \tag{7}$$

where $\langle \cdots \rangle$ represents an ensemble average over many trajectories with initial action $I(0)$. The diffusion out to the regular region is, however, impeded by barely broken KAM tori (cantori) further out in the chaotic layer (see Figs. 2 and 3). ''Cantorus'' refers to the remnants of an irrational wind-

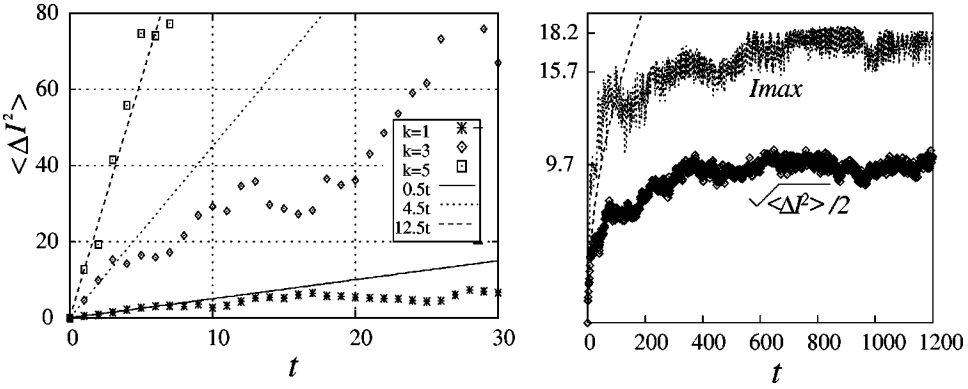

FIG. 2. (left) Classical diffusion in the whisker map, $\lambda=10$: $\langle \Delta I^2 \rangle$ for a set of initial conditions with vanishing action. The initial slopes agree with Eq. 7. (right) Later, diffusion is impeded by cantori. This graph shows the maximum action in the distribution, $\lambda=10, k=2$. Also a scaled square root of the dispersion in action is shown. The dashed line corresponds to unimpeded diffusion given by Eq. (7).

ing number invariant manifold at, or just above, the critical nonlinearity parameter k_c at which the manifold breaks up. At the break-up parameter, the KAM surface acquires a scale-invariant fractal structure. It is an invariant set with an infinite number of infinitesimal gaps [5,19] and it presents partial barriers to motion for a nonlinearity parameter k_s larger than k_c, invalidating the diffusion picture. (Of course, for smaller k_s they are complete barriers to transport, and for much larger k_s the cantori disintegrate and diffusion may proceed rapidly, as in the chaotic region). Greene found [20] that the last surviving KAM curves for the standard map [Eq. (3)] have winding number $\pm(\gamma \pm m)$ where $\gamma=(\sqrt{5}+1)/2 \approx 1.618$ is the golden mean and m is an integer. This curve remains robust as the magnitude of the standard map parameter k_s increases from 0 to $k_c=0.9716354\cdots$ [20], when it breaks up and global chaos sets in. The golden mean (and its integer relatives) is, in a sense, the ''most irrational'' number: its continued fraction representation is the slowest to converge. Other irrational winding numbers w correspond to trajectories that lie on an invariant curve under small perturbations but they break up at parameters $|k_c^w|<k_c$. See Refs. [8,9,13,20,5–7,21] for more detail.

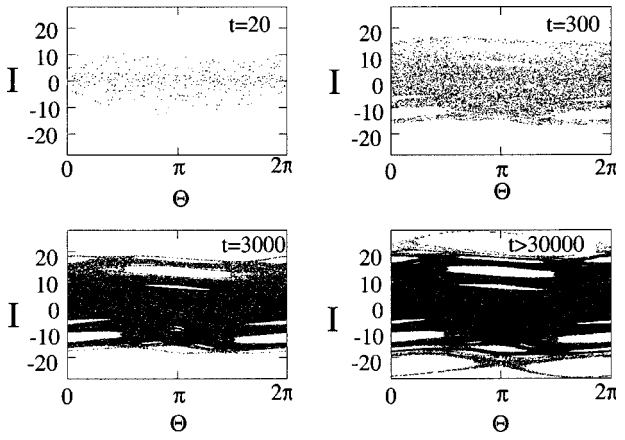

FIG. 3. Classical evolution of 20 points initially with random θ and $0<I<1.\lambda=10, k=2$. The borders of the distribution at each time shown are at cantori: $t=20$ shows the cantorus at winding number $4-\gamma^{-2}$, $t=300$ shows that at $4+\gamma^{-2}$; $t=3000$ shows that at $5-\gamma^{-2}$ (see text). Finally ($t>30\,000$) the outermost cantorus is penetrated and the distribution spreads to the border with the regular region.

For the whisker map the strongest restraints on diffusion in the chaotic layer arise from cantori with winding number $\pm(\gamma \pm m)$, for integer m. The unperturbed whisker map winding number is $w_o=1/r_o$, where

$$r_o(I)=\frac{1}{w_o}=\frac{\lambda}{2\pi}\ln\left|\frac{c}{I-I_o}\right|. \tag{8}$$

Typically there are several cantori corresponding to winding numbers $w=m\pm\gamma^{-2}$ which are ''effective'' within the chaotic layer, with varying degrees of ''brokenness.'' (Note that $\gamma^{-2}=1-\gamma^{-1}=2-\gamma\approx 0.382$.) Those near the outer border of the chaotic layer are close to critical and present much stronger impediments to diffusion than those further inside the layer; this is as suggested by the local standard map parameter at the cantori [Eq. (5)]. For example, in Figs. 2 and 3, there are three cantori evident, corresponding to inverse winding numbers r of $4-\gamma^{-2}$, $4+\gamma^{-2}$, and $5-\gamma^{-2}$ at $|I-I_o|\approx 9.7, 15.7, 18.2$, respectively. These are the values of unperturbed actions: the cantori are actually curved, as is evident in the phase-space pictures. The classical distribution is slowed at each cantorus for some time, which is longer the further out the cantorus is, before escaping finally into the stochastic layer. Ultimately a trajectory fills the phase space (except for the islets of stability) up to the regular region (Fig. 3). It is also important to note that each cantorus has a ''width'' which represents the range in action around the cantorus in which the transport is slowed down due to closely neighboring irrationals (see also Sec. III B).

As k increases, the cantori become weaker and the inner ones may disappear as new ones appear at the growing edge of the chaotic layer. In Fig. 4 we have zoomed in on the border between the chaotic and regular regions in the whisker map with parameters $\lambda=10, k=1.77$. These parameters conspire to give a critical cantorus at winding number $5-\gamma^{-2}$ at action $I=18.7$ (the parameter $I_o=0.5$). Although the cantorus itself is not visible in this picture, which is limited by the number of points iterated, what one can see clearly are the resonance island structures embracing where the cantorus would be. One can make out a period 2, period 3, period 5, period 8, and period 13 chain, alternating between the two sides of the cantorus. Of course this structure is not unique to cantori in the whisker map: the periodic orbit structure occurs around generic cantori. These periodic orbits

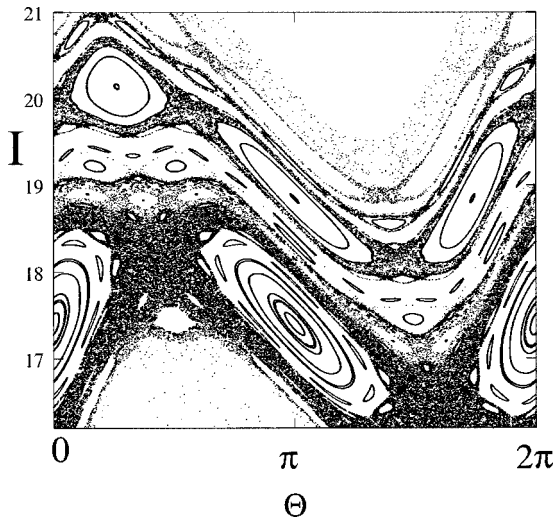

FIG. 4. Classical phase-space near a near-critical cantorus at the border of the stochastic layer.

are the ''convergents'' to the KAM surface; they have winding numbers which are successive truncations of the continued fraction representation of the irrational winding number associated with the KAM. For the golden mean, the convergents have period given by the Fibonacci sequence $F_0=0, F_1=1, F_{i+1}=F_i+F_{i-1}$ with winding numbers F_i/F_{i+1}. As $i\to\infty$ this number approaches γ. The figure does not have enough points to resolve the structure beyond the 13th level.

The periodic orbit convergents are in a sense responsible for the fractal structure at criticality and the scale invariance near a cantorus. (In fact it was a study of their stability as a function of the nonlinearity parameter which led Greene to his result regarding the destruction of the last KAM surface in the standard map [20]). There is an extensive literature on the scaling behavior and renormalization group theories (both analytic and numeric [8,9,6] near the cantorus to describe the ''structure at all scales.'') The behavior at criticality has universal characteristics: near the critical break-up parameter for other irrational winding numbers and for other maps one finds the same scaling exponents [8] and the same universal map. Thus the scaling relations controlling the classical (and quantum) dynamics near a cantorus are universal. We let μ represent the distance from criticality [e.g., for the standard map Eq. (3), $\mu=|k|-k_s=\Delta k$]. Then, asymptotically, a map in (θ,p) near a generic cantorus is invariant under the rescaling [8,9,6]

$$\begin{aligned} \mu &\to \delta\mu, \\ \Delta\theta &\to \alpha\Delta\theta, \\ \Delta p &\to \beta\Delta p, \\ n=F_{r+1} &\to F_r \sim n/w, \end{aligned} \tag{9}$$

where $\delta\approx 1.628$ is the scaling exponent for the nonlinearity parameter μ; $\alpha\approx -1.41(-1.69)$ near $\theta=\pi(0)$ and $\beta\approx -3.07(-2.56)$ near $\theta=\pi(0)$. The last relation expresses time rescaling, n being the number of iterations of the map, with scaling exponent given by the irrational winding number of the KAM, e.g., for the golden mean torus of $w=\gamma\approx 1.618$. Note that the values of α and β correspond to those at the dominant (subdominant) symmetry line; these are lines of fixed points of the involutions T_1 and T_2 whose product gives the original map (see Refs. [8,6]). The subdominant symmetry line tends to cross a hyperbolic point of each periodic convergent, whereas the dominant line contains an elliptic point of each periodic convergent. The essential point here is that for the standard map of the form in Eq. (3) for $I>I_o$ and $k_{\rm eff}>0$ the dominant and subdominant symmetry lines are at $\pi(0)$, respectively. For $I<I_o$ (where $k_{\rm eff}$ is negative), the dominant and subdominant symmetry lines are at $0(\pi)$, respectively, and the values of α and β at 0 and π should be switched. Notice that at both the subdominant and dominant symmetry lines, the product of the phase-space scalings $\alpha\beta\approx 4.34$.

A. Flux through a cantorus

Perhaps the most important aspect of classical behavior near barely broken tori, for our purposes, is the flux across a cantorus. This is the flux ΔW swept across the cantoral gaps in one iteration of the map. The ''turnstile'' construction to compute this is described in Refs. [6,13]. The flux through the cantorus ΔW follows a scaling relation that is not difficult to guess from Eqs. (9):

$$\Delta W(\mu)\to(\alpha\beta)^{-1}\Delta W(\delta\mu), \tag{10}$$

where $\mu=\Delta k_s=|k_s|-k_c$. This can be expressed as

$$\Delta W(\mu)\propto\mu^{\eta} \tag{11}$$

with $\eta=\ln\alpha\beta/\ln\delta\approx 3.01$. That the flux scales as $\sim(\Delta k_s)^3$ holds for a surprisingly wide range of k_s: for the standard map, the authors in Ref. [21] show numerically that the diffusion in action goes as $(\Delta k_s)^3$ up to $k_s\sim 2.5$.

In Ref. [5], ΔW for the golden mean cantorus of the standard map was computed as the limit of that for high-order periodic orbit convergents. From that study the proportionality factor in Eq. (11) is deduced:

$$\Delta W^{kr}(k_s)\approx 0.7(\Delta k_s)^3. \tag{12}$$

Appealing to universality, we expect that the dependence on the nonlinearity parameter (i.e., the scaling exponent η) holds for general one-parameter maps and for cantori at other noble winding numbers, however, probably with a different proportionality constant.

We exploit the fact that the whisker map is locally a standard map to calculate the cantoral flux. Generalizing Eqs. (4) and (5) to the neighborhood of a cantorus, I_r is replaced by the action at the cantorus rather than at the fixed point. Although we cannot strictly write the whisker map as a local standard map, except close to a fixed point, there certainly is a sense in which we can associate an effective standard map parameter and corresponding phase-space scalings anywhere inside the stochastic layer. We have

$$\Delta W = \frac{|I_{ct}-I_o|}{\lambda}\Delta W^{kr}\left(\frac{\lambda k}{|I_{ct}-I_o|}\right)$$

$$\approx 0.7\frac{|I_{ct}-I_o|}{\lambda}\left(\frac{\lambda k}{|I_{ct}-I_o|}-k_c\right)^{\eta} \quad (13)$$

$$\approx \frac{0.7ce^{-2\pi(r\pm\gamma^{-2})/\lambda}}{\lambda}$$

$$\times(\lambda kce^{2\pi(r\pm\gamma^{-2})/\lambda}-k_c)^{\eta}, \quad (14)$$

where the last line specializes to the case of a cantorus at inverse winding number $r\pm\gamma^{-2}$.

There is another way to derive the whisker cantoral flux from a formula derived in Ref. [13]. Letting $\Delta W_{p/q}(R^*)$ denote the flux through the periodic orbit of winding number p/q, one may write

$$\Delta W \approx 0.37\Delta W_{p/q}(R^*)\left(\ln\frac{R_{p/q}}{R^*}\right)^{\eta} \quad (15)$$

where R is the residue of the p/q periodic orbit and R^* is its value at criticality [20]. [$R=(2-\mathrm{Tr}\,M)/4$ where M is the tangent map of the periodic orbit.] There, it is also asserted that for a cantorus sandwiched between two periodic orbits of neighboring rationals (i.e., $p'q-pq'=\pm 1$) which have residues of significantly different size, one may replace the logarithm in Eq. (15) with the combination weighted by the inverse ''distance'' from the resonance to the cantorus. For example, for a cantorus with unperturbed inverse winding number $r\pm 1/\gamma^2$, we have $\Delta W\approx 0.37\Delta W_r(R^*)[(1/\gamma)\ln(R_r/R^*)+(1/\gamma^2)\ln(R_{r\pm 1}/R^*)]^{\eta}$. It is straightforward to calculate the components of this expression for cantori in the whisker map using the fixed points for the periodic orbit pivots on the right-hand side. One obtains, for a cantorus at inverse winding number $r\pm 1/\gamma^2$

$$\Delta W \approx \frac{0.7ce^{-2\pi r/\lambda}}{\lambda}\left[\frac{1}{\gamma}\ln\left(\frac{\lambda kce^{2\pi r/\lambda}}{k_c}\right)\right.$$

$$\left.+\frac{1}{\gamma^2}\ln\left(\frac{\lambda kce^{2\pi(r\pm 1)/\lambda}}{k_c}\right)\right]^{\eta}. \quad (16)$$

This was also obtained in Ref. [14].

We notice this is *almost* exactly the same as our earlier formula (14): the terms in the large parentheses may be combined as

$$\ln\left(\frac{\lambda kce^{2\pi(r\pm\gamma^{-2})/\lambda}}{k_c}\right)$$

which gives the same term as that taken to power η as in Eq. (14) once the argument of the logarithm is expanded around 1. The only difference with Eq. (14), is then an overall factor of $e^{\pm 2\pi/(\lambda\gamma^2)}$. The difference presumably comes about because in the formula (16) only the closest resonance is accounted for in the prefactor, but in our formula (14), an effective weighted combination from both resonances occurs from the local standard correspondence. We are thus inclined to trust (14) more when calculating the flux. In Sec. III B we shall provide numerical evidence supporting our approximation.

B. Scaling relations in quantum mechanics

We end this introductory part of the paper by a brief discussion on what happens to the scaling relations in a quantized system. The effect of scaling on quantum mechanics has been discussed in the literature, e.g., Ref. [10,15,22]. To first order, the scaling properties carry over to the quantized motion near a cantorus, provided Planck's constant is also scaled: the relation [10,15]

$$\hbar\rightarrow|\alpha\beta|\hbar \quad (17)$$

joins Eqs. (9). However, as time evolves, $\hbar$ effectively gets scaled to larger and larger values and eventually becomes larger than the scaling region [10]. At this time, scaling breaks down as $\hbar$ is too large to resolve the structures which give rise to scaling. The breakdown happens at the time t^* which scales as $t^*\sim\hbar^{-1/\gamma}$, $\gamma=\ln|\alpha\beta|/\ln\omega\approx 3.05$. In [10] it is argued (numerically and also semiclassically) that this is also the time scale when quantum effects such as interference begin to become important. A consequence of this for quantum diffusion in the kicked rotor at $k>k_c$ is the onset of localization. Quantum dynamics follows the classical diffusion, scaling with k as does the flux [$\sim(\Delta k)^3$], but begins to deviate at times scaling with $\hbar$ as $t^*\sim\hbar^{-1/\gamma}$. We refer the reader to Ref. [10] for graphs of this behavior in the kicked rotor. There is some diffusion in action after t^*, albeit slower; the system does not completely localize in the sense of $\langle\Delta p^2\rangle$, not reaching a steady state until much later. The approach to complete localization is not a simple one.

III. QUANTUM LOCALIZATION IN THE CHAOTIC LAYER

A. Preliminary observations

We examine the long-time properties of the quantized map *via* the time-averaged probability of being in final state $|f\rangle$ having started in initial state $|i\rangle$:

$$P(f,i)=\lim_{T\rightarrow\infty}\frac{1}{T}\sum_{t=0}^{T}|\langle f|U^t|i\rangle|^2$$

$$=\sum_n|\langle f|n\rangle|^2|\langle i|n\rangle|^2, \quad (18)$$

where in the last line the sum goes over the quasienergy eigenstates. U is the one-step time evolution operator for the map

$$U=e^{-i\lambda(I-I_o)[\ln|c/(I-I_o)|+1]/\hbar}e^{ik\cos\theta/\hbar}.$$

For example, in action representation [14,23],

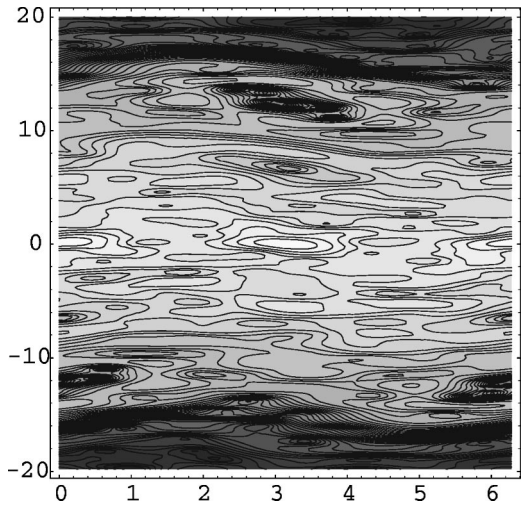

FIG. 5. Husimi plot with logarithmic contours for the time-averaged probability in the whisker map with $\lambda=10, k=2, \hbar=0.2, I_o=0.1$. Initial state is a coherent state centered at $\theta=\pi, I=0$.

$$\langle I_f|U|I_i\rangle=\frac{\hbar}{2I_c}e^{-i\lambda(I_f-I_o)[\ln|c/(I_f-I_o)|+1]}\times\sum_{p=0}^{2(I_c/\hbar)-1}e^{-i\pi(I_f-I_i)p/I_c+ik\cos(p\pi\hbar/I_c)/\hbar}. \quad (19)$$

There are two particularly useful representations in which to study this object: one is a phase-space representation (a Husimi plot), the other is action space. The phase-space representation helps us to understand qualitative aspects of the localization. We take circular coherent states

$$\alpha(\theta)=\exp[-(\theta-\theta_\alpha)^2/2\hbar+iI_\alpha\theta/\hbar]/(\pi\hbar)^{1/4}$$

as final and initial states in Eq. (18). θ_α and I_α denote the center coordinates of the coherent state. Figure 5 is a contour plot of the logarithm of the time averaged density in a whisker map of $\lambda=10, k=2, \hbar=0.2$ where the initial coherent state is centered at $\theta=\pi, I=0$ (I_o is 0.1). The chaotic layer covers almost all of the shown phase space for these parameters. The shading reflects the magnitude, with light being high and dark low, however, it is important not to be misled by regions of dense contours which make the region look dark when it is not. Such regions indicate a rapid exponential change in the magnitude of the probability. We see structures which we recognize from the corresponding classical phase space: islets of stability centered at $|I-I_o|=(12.3, 6.6)$ and $\theta=\pi(0)$ at $|I-I_o|>0(<0)$, respectively. The shading out from the initial state indicates a gentle exponential decay in the deep stochastic layer. This meets a series of curved precipices, one set at $|I-I_o|\sim 10$, another set at $|I-I_o|\sim 16$, and yet another at $|I-I_o|\sim 18$. The precipices coincide with the cantori in the stochastic layer and indeed their shapes in the Husimi plot resemble their shapes in the classical phase space, Fig. 3.

A more efficient way than Eq. 18 to calculate the time-averaged probability in action involves performing a forward and backward fast-fourier transform at each time step [24]:

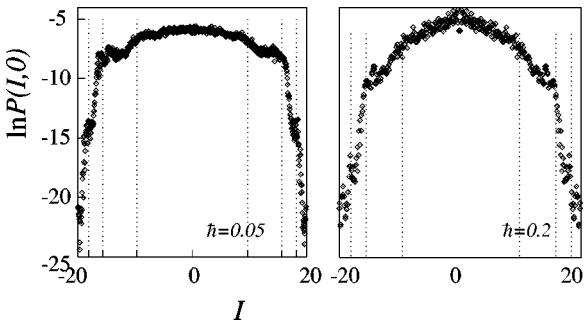

FIG. 6. $\lambda=10, k=2, \hbar=0.05$ and $0.2, I_o=0.1$, logarithm of the time-averaged probability in action $I=0$. The dashed lines indicate the cantori (see text).

$$\langle I_f|U^t|\psi_i\rangle=\sum_j\langle I_f|U|I_j\rangle\langle I_j|U^{t-1}|I_i\rangle$$
$$=\frac{\hbar}{2Ic}e^{-i\lambda(I_f-I_o)(\ln|c/(I_f-I_o)t|+1)}\times\sum_{p=0}^{2I_c/\hbar-1}e^{-i\theta_pI_f/\hbar}e^{ik\cos\theta_p/\hbar}\times\sum_{j=-I_c}^{I_c}e^{-i\theta_pI_j/\hbar}\langle I_j|\psi_i(t-1)\rangle, \quad (20)$$

where $\theta_p=p\pi\hbar/I_c$. The squared norm of this is then summed over all times. For the computations we used the program FFTW [25], which held true to its name (''fastest Fourier transform in the West'').

The logarithmic plots 5 and 6 indicate steep exponential decay at the cantori. Classically we observed that (noncritical) cantori quench the fast diffusion deeper in the layer; trajectories take many iterations to get out, but at long times they roam uniformly all over all the connected chaotic phase space. In the quantum case the transport is much more severely impeded, the probability of long-time penetration being exponentially suppressed. The eigenstates are exponentially localized in action and consequently transport across the layer is much impeded. Typically, the further out in the stochastic layer the cantorus is, the steeper the ''cliff'' in the logarithm of the time-averaged probability (see for example, Fig. 6).

Cantori acting as exponential barriers in quantum mechanics have been discussed before [10,11,13,14]. The localization there results from Planck's constant exceeding the flux through the cantorus: the quantum mechanics sees a closed surface rather than a broken cantorus. This gives a barrier, but not an impenetrable one. The quantum system can tunnel to get across it. We give this phenomenon the name ''retunneling'' to distinguish it from ordinary classically forbidden tunneling. (The name ''retunneling''is appropriate, because quantum mechanics sets up a blockade where none exists classically and then tunnels through it.)

A major new point in this work is that cantori can also be exponential barriers when *h* is *smaller* than the gaps, as we shall show in Sec. III B. This is due to a dynamical localization mechanism: when the classical mechanics diffuses sufficiently slowly, the corresponding quantum mechanics lo-

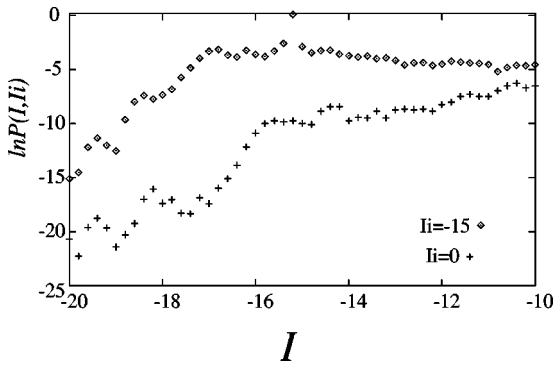

FIG. 7. $\lambda=10, k=2$ and $\hbar=0.2$, time-averaged probability in action space, where the initial action is $I=-15(\diamond)$ and $I=0(+)$.

calizes. Dynamical localization also occurs deep in the chaotic layer; below we discuss similarities and differences of such localization with dynamical localization at cantori. Thus there are two quite different mechanisms which are responsible for the exponential decay at cantori; we discuss them in some detail in Secs. III B and III C. Studying the $\hbar$ dependence of the time-averaged probability (and also the explicit time dependence) guides us in this study and indicates which mechanism is at work. Our main contributions, in addition to pointing out the existence of a dynamical localization mechanism at cantori, are to an understanding of the retunneling mechanism $\hbar$ dependence away from criticality, and a new argument for the previously discovered $\hbar$ dependence at criticality.

As remarked above, the contours of the Husimi measure of transport near a cantorus from an initial action well inside the central chaotic zone follow the shape of the cantorus. This is consistent with the observation in Ref. [21] of the classical motion near a cantorus in the kicked rotor: the classical trajectories in a strip around the cantorus tend to follow curves parallel to the cantorus, with a much slower diffusion in a direction normal to the cantorus. Our Husimi plots suggest that the quantized system has a related property: the localization mechanism (be it dynamical or retunneling) respects the local curvature in phase space that k gives to the convergents near a cantorus. We expect that the exponential decay occurs not exactly at the golden mean cantorus but in a strip around it, due either to dynamical localization resulting from slow classical diffusion or from retunneling through other cantori in the strip whose gaps are smaller than $\hbar$. This is reinforced by both the Husimi plots and the action plots.

Inspecting the time-averaged probability in action, Fig. 7, it is important to bear in mind both the curvature near the cantorus and the effective width around it within which the decay occurs, as described above. Monitoring action transport corresponds to initiating and checking horizontal lines in the phase plane. Such a constant action line may initially touch the curved cantorus band tangentially at one point, affecting where the exponential decay begins. In Fig. 7 we focus on the logarithm of the time-averaged probability near the cantorus at inverse winding number $4+\gamma^{-2}$ in the whisker map with $\lambda=10, k=2$. When the initial state is deep in the chaotic layer at initial action $I=0$, a sharp exponential decay begins at $I=-16$ whereas the onset of sharp decay for starting at initial action $I=-15$ is at $I=-17$. The value $I=-16$ is the extremal action of the inner end of the cantoral

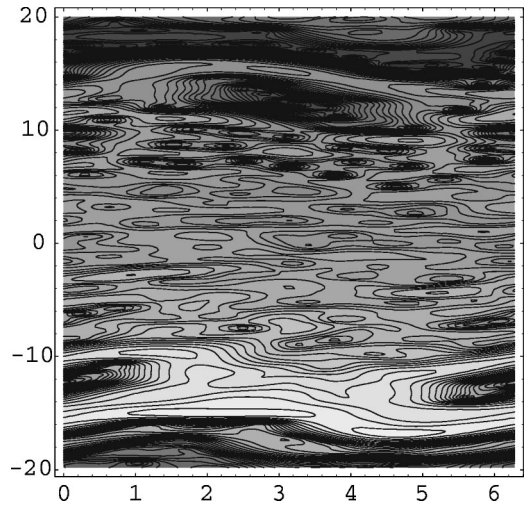

FIG. 8. $\lambda=10, k=2, \hbar=0.2$, initial action state $I=-15$.

strip (not the extremal edge of the cantorus but rather, of the strip surrounding the cantorus). It is thus the curvature of the cantorus together with the width of the cantoral strip that determine the onset at $I=-16$. The Husimi plot of Fig. 5 supports this. Starting with an action state at $I=-15$ cuts across a range of the ''natural'' curved states in the cantorus band so that the quantum time-averaged probability shows almost no decay until a limiting, extremal action that can be reached by any of the curved cantorus localization bands that the initial action state lies on. This is further elucidated by the Husimi plot of the time-averaged propagator having started in the action state $I=-15$, as shown in Fig. 8. If the initial action is changed in such a way that it still touches the cantoral band in some range of angle, the limiting value of the action changes correspondingly. The onset of the exponential decay is at this limiting action, *not* at the extremal I of the cantorus. This point has been somewhat neglected in the kicked-rotor literature.

B. Dynamical localization at cantori

The concept of dynamical localization in *hard chaotic* systems came to light in the 1980's [26–29], where the standard map at large kick strength was studied. The energy and momentum were found to be bounded at large times, in contrast to the diffusive classical behavior. The quantum mechanics follows the classical behavior up to the ''break'' time, or quantization time, $t_b \sim h/\delta E$, when all the quantum states are resolved and the motion becomes quasiperiodic. (Of course since δE depends on h this relation does not mean that the quantization time scales linearly with h.) Quantum interference leads to exponentially localized states. We refer the reader to Refs. [27,30] for a simple argument (based on the kicked rotor system) which predicts the localization length: the probability distribution of a state centered at action I_{cn} goes as

$$e^{-2\hbar(I-I_{cn})/D}, \tag{21}$$

where D is the classical diffusion constant. In fact one can check that this relation holds in the *deep* chaotic layer in the whisker map. [The dynamical localization occuring there satisfies this relation provided the localization length in action

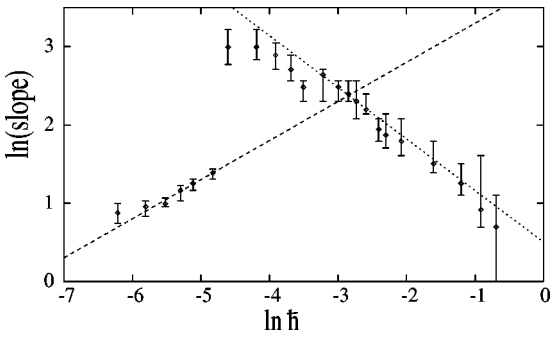

FIG. 9. Slopes at an inner cantorus (winding number $1+\gamma^{-2}$) as a function of $\hbar$. The classical parameters are $\lambda=5,k=1.5$. The effective standard map parameter is $k_{\rm eff}=1.32$. The dashed lines have slopes 0.5 and -0.66 (see text).

$k^2/(2\hbar)$ is small enough that the distribution does not encounter a cantorus before this is achieved.]

Classical motion in the scaling region near a noncritical cantorus is a slow diffusion in action, the diffusion constant being proportional to the flux transported across the cantorus, ΔW [Eq. (14)]. We may then expect that the quantum counterpart displays dynamical localization, similar in principle to that in the deep chaotic layer. However, the details are quite different: it was shown in Ref. [10] that the onset of localization happens at a time scaling similar to $\hbar^{-1/\gamma}$ and the subsequent approach to complete localization shows a more complicated dependence on time than in the strong chaotic case. We refer the reader to Sec. II B and the references there; in particular to Ref. [10]. The simple argument leading to Eq. (21) for the localization length in the strong chaotic case no longer holds and as a consequence the $\hbar$ and ΔW dependence of the localization length are more complicated.

The slope of the logarithm of the time-averaged propagator gives the exponential decay factor and is inversely related to the localization length. In Fig. 9 we have plotted the logarithm of this slope at an inner cantorus of the whisker map with $\lambda=5$ and $k=1.5$. This cantorus is at inverse winding number $1+\gamma^{-2}$ and corresponds to the unperturbed action ~ 5.68. The extremal value of the cantorus is at ~ 6.4. The effective standard map parameter for this cantorus is $k_{\rm eff}=1.32$.

A typical graph of the time-averaged probability near this cantorus is shown in the top graph of Fig. 10, where the initial state is at 4. Most initial conditions decay with about the same slope at the cantori and the error-bars in Fig. 9 account for the variation. Exceptions are when the initial state lies well in the cantoral strip (see Sec. III A) or when tunneling interactions into resonances around the cantorus enhance the probability of being found there. The slope recorded in Fig. 9 is that at the outer edge of the cantorus.

For $\ln\hbar<-4$ the slopes increase more slowly than in the strongly chaotic case, going as $\hbar^{\rho}$ where $\rho<1$, rather than as $\hbar$, as in the deep stochastic layer. ρ is close to 0.5 in the case shown. We find ρ depends on $k_{\rm eff}$ but is always smaller than 1. For very small $\hbar$ the localization length would be too large to be resolved within the cantoral width. For larger $\hbar$, the local slopes at the cantorus reverse behavior and begin to

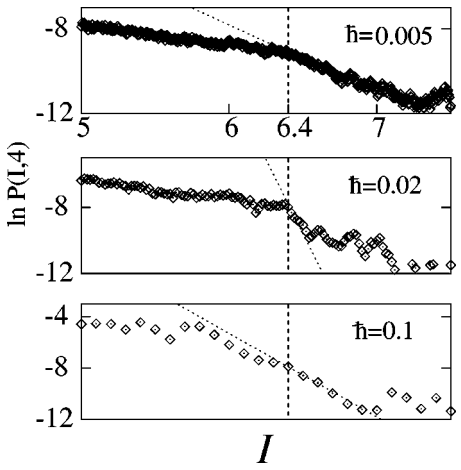

FIG. 10. Logarithm of the time-averaged probability near the cantorus at winding number $1+\gamma^{-2}$, whose outer edge is at $I=6.4$. The slopes are 3.2, 18, and 6.5 respectively. Note the scale differences on the vertical axis.

decrease as $\hbar$ increases. This heralds the changeover from dynamical localization to re-tunneling, to be discussed in the next section.

We note that our small $\hbar$ results are consistent with the findings in Ref. [31]. There the authors extract a scaling function for decay of wavefunctions across resonance zones from a quantum renormalization map. Using an argument based smaller values of $\hbar$ resolving more of the classical phase space structure, hence higher order periodic convergents, they explain the qualitative behavior of the $\hbar$ dependence of the exponential decays within the framework of their renomalization map.

We can examine this in the time domain also, as shown in Fig. 11 and the $\hbar=0.001,0.008$ traces in Fig. 12. The initial state is at $I=0$ and all the quantum curves as well as the classical initially diffuse out at the classical rate $k^2/2$ (see Fig. 12). We notice that for small enough values of $\hbar$ the quantum dynamics follows the classical into the cantoral region. This is the $\hbar$ regime we are currently discussing. The quantum states then localize, falling away from the classical distribution at various times after that. We shall come back to these plots shortly.

As the approach to localization is complicated we cannot predict the ΔW dependence of the localization length other

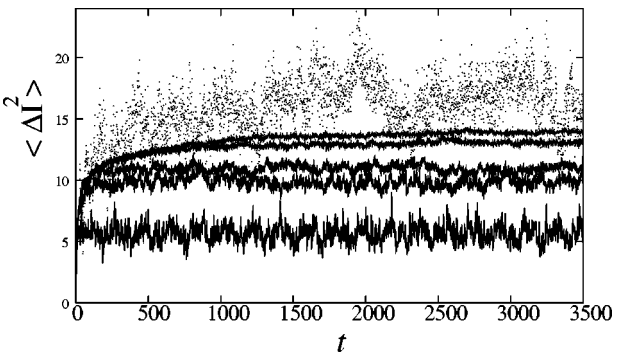

FIG. 11. $\langle\Delta I^2\rangle$ for the whisker map, $\lambda=5,k=1.5$. The dots represent a classical average, the curves from the top down are at $\hbar=0.001,0.002,0.008,0.02,0.1$, respectively.

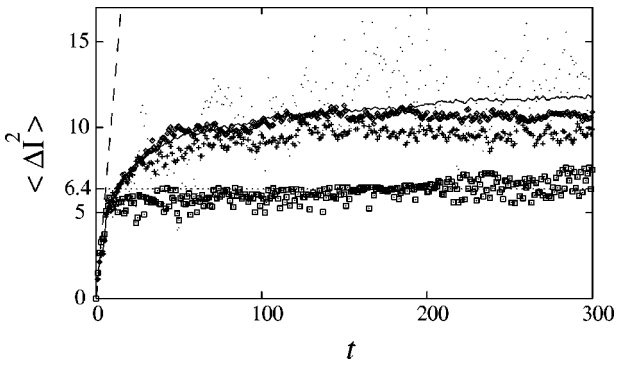

FIG. 12. $\langle \Delta I^2 \rangle$ for the whisker map, $\lambda = 5, k = 1.5$. The dots represent a classical average. The curves from top down are at $\hbar = 0.001$ (line), $0.008(\diamond), 0.02(+)$. The $\square$ represents the maximum action of the classical distribution. The dashed line indicates the initial diffusion of all quantum and classical curves, with diffusion constant 1.125.

than to expect that it goes as some positive fractional power of the flux. We have checked that this is true. Recall that locally the whisker map is a kicked rotor [Eq. (3)]. In Fig. 13 we have plotted the slopes of the logarithm of time-averaged probability for the kicked rotor at nonlinearity parameter $k_{\text{eff}} = \lambda k / |I_{ct} - I_o| = 1.32$ corresponding to the whisker parameters $\lambda = 5, k = 1.5$ at the cantorus at $1 + \gamma^{-2}$. We notice that the quantum kicked rotor slopes are roughly a factor of 1.3 higher than those in the whisker (in the dynamical localization regime). This supports our formula (14) over that in Ref. [14] and Eq. (16): the flux through the whisker cantorus is that through the corresponding kicked rotor times $|I_{ct} - I_o|/\lambda = 1.14$ whereas that of Eq. (16) says that the factor relating the two is $|I_r - I_o|/\lambda = 0.7$.

Our main observation in this section is the $\hbar^\rho$ dependence of the logarithm of the time-averaged transport probability in the vicinity of the cantoral strip, with ρ being a positive fraction when h is smaller than the flux. This supports our assertion and qualitative observations in the previous sections that cantori can act as exponential barriers when $\hbar < \Delta W/\pi$, due to a dynamical localization mechanism. The dependence found in the time domain is consistent with the interpretation that it is a dynamical localization effect.

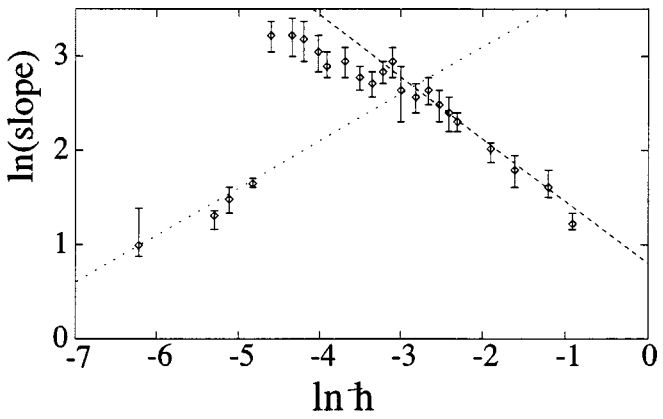

FIG. 13. Slopes of the quantum kicked rotor, $k_s = 1.32$. The dashed lines have slope 0.5 and -0.66.

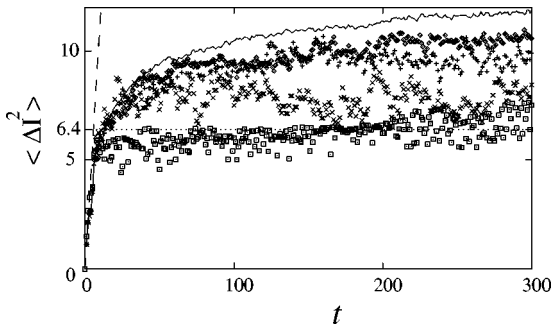

FIG. 14. As in Fig. 12 but with the quantum data being at $\hbar = 0.001, 0.01, 0.02, 0.05$, respectively.

C. Retunneling

At a larger value of $\hbar$, the time-averaged probability graph develops a sharp kink at the cantorus (lower two pictures of Fig. 10); see also Fig. 9 for $\log \hbar > -4$. This signifies the beginning of a different type of localization mechanism at the cantorus. Quantum diffusion cannot happen when $h/2$ is larger than the flux across a cantorus ΔW: the quantum mechanics can no longer resolve the gaps (turnstiles) in the cantorus when $\hbar > \Delta W/\pi$. In fact we first see a kink when $\hbar \approx 0.01$ and indeed $\Delta W/\pi = 0.01$ using our formula (14). In Fig. 9, the slopes now decrease as $\hbar$ increases for $\hbar > 0.01$, whereas they increase as $\hbar$ does for $\hbar$ below 0.01. This supports the idea that it is a different localization mechanism: As the system becomes less classical (i.e., larger $\hbar$) any dynamical localization and retunneling effects become stronger. In dynamical localization the system becomes more strongly localized as $\hbar$ increases (so slopes increase); in the latter case more tunneling means more transport as $\hbar$ increases (so slopes decrease). The slopes plotted in the figures are again the *local* slopes at the cantorus. (Of course immediately around the cantorus there are other cantori with $\hbar > \Delta W$ and also resonance chains. This affects the overall slope or transport property in the region. In this figure we are concerned only with the local slope at the cantorus.)

We can see the distinction between exponential decay due to dynamical localization and tunneling in the time domain also. First consider again Fig. 11. It is clear that quantum mechanics at $\hbar = 0.1$ does not manage to diffuse into the inner cantoral region, as it collapses at $\langle \Delta I^2 \rangle \approx 5.7$ just as the corresponding classical distribution has reached the cantoral region. To see whether the smaller $\hbar$'s manage to penetrate the cantorus (without having to resort to tunneling over long times), we focus in on shorter times in Figs. 12 and 14. Here we have also plotted the maximum of a classical distribution of points with initial $I = 0$ and evenly spaced in angle. The dashed line at 6.4 is the outer edge of the cantorus at $1 + \gamma^{-2}$: the classical distribution gets held up by this cantorus between about $t = 40$ and $t = 200$. In the range of time plotted in these two figures, the quantum spread at $\hbar = 0.001$ follows the classical average: in this time regime we can think of this curve as representing the classical average. (It in fact penetrates this cantorus and then localizes.) The quantum spread at $\hbar = 0.008$ appears to follow the classical into the cantoral region and then falls away and localizes shortly before about $t = 200$. It localizes within the cantoral strip (with the corresponding localization length in the time-averaged picture as

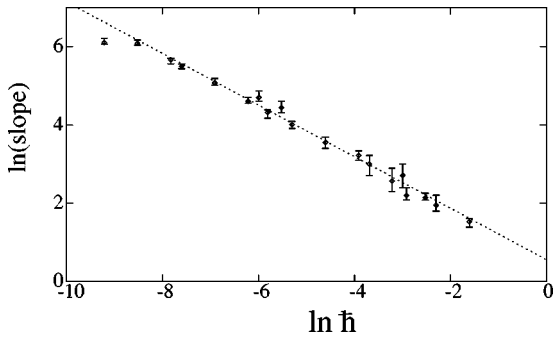

FIG. 15. Slope at the near-critical cantorus $k_{\rm eff}=0.98$ (winding number $2-\gamma^{-2}$ with $\lambda=5, k=1.5$). The slope of the dashed line is -0.66.

plotted in Fig. 9). However, at $\hbar=0.02$ the dynamics never makes it to the cantoral strip: the graph falls away from the classical average (and the smaller $\hbar$ quantum plots) when the classical maximum reaches the edge of the cantorus. [$\langle \Delta I^2\rangle$ can still grow somewhat after that time, when the highest actions in the evolved distribution reach the cantorus. Subsequently, more of the distribution can diffuse and so the expectation value $\langle \Delta I^2\rangle$ grows.] Figure 14 shows a similar plot for different $\hbar$'s. The $\hbar=0.01, 0.02, 0.05$ curves fall away from the $\hbar=0.001$ (and the classical) when the classical maximum strikes the outer edge of the cantorus. That they all fall away at the same time is another indication that the cantorus presents a barrier to diffusion through which they can only tunnel. (If it was a dynamical localization effect that we were seeing, different $\hbar$'s would fall away at different times.)

From Figs. 9 and 13 we observe that the $\hbar$ dependence of the retunneling does not go as $e^{-a\Delta I/\hbar}$ as in ordinary tunneling across a KAM torus or a potential barrier. Rather, when $\hbar$ is somewhat bigger than ΔW it fits a dependence more as $e^{-a\Delta I/\hbar^{\sigma}}$ where σ is a fraction close to 0.66. When $\hbar \simeq \Delta W$ or a bit larger, the dependence is weaker. In Fig. 15 we have considered a cantorus closer to criticality: this is one further out in the chaotic layer of the same whisker map. It has inverse winding number $2-\gamma^{-2}$, with unperturbed action 7.64 and effective standard map parameter $k_{\rm eff}\approx 0.98$. Again, the $\hbar$ dependence of the retunneling in this near-critital cantorus is close to $e^{-a\Delta I/\hbar^{0.66}}$. At *criticality*, this exponent has been previously found in the quantum kicked rotor, but here we are claiming a wider applicability, which we now discuss.

For a *critical* cantorus ($\Delta W=0$) of the kicked rotor it has been found numerically that the tunneling probability goes as $\hbar^{-\sigma}$ where $\sigma\approx 0.66$ [11]. In Ref. [10], this exponent is shown to be related to scaling exponents in this region. We give a different but related argument to that in Ref. [10]: one based on perturbation theory. Consider the basis of deformed action states, which have curvature in phase space following the curvature of the nearby cantorus. Let us label these states by their extremal value of action $|I_m^{\rm ex}\rangle$. Then, in the neighborhood of a near-critical cantorus, a transition between two such curved states $|I_m^{\rm ex}\rangle$ and $|I_n^{\rm ex}\rangle$ is very weak; as we have seen in the Husimi plots, the transition is exponentially small, and in the classical picture, trajectories follow along the curve but transport between different curves is very slow. In such a case, we might expect a perturbation matrix element could well give the transition probability amplitude and hence the tunneling rate across the cantorus. If v is the appropriate perturbation potential for this, then

$$\langle I_m^{ex}|v|I_n^{ex}\rangle = v(\Delta I,\hbar,\Delta k) = \beta^{-r} v(\beta^r \Delta I, |\alpha\beta|^r \hbar, \delta^r \Delta k), \tag{22}$$

where in the first step we have expressed the amplitude in terms of all the parameters it could depend on and in the second step we have used scaling properties [see Eqs. (9) and 17)]. We use the shorthand ΔI for $I_m^{\rm ex}-I_n^{\rm ex}$. Let us first consider a critical cantorus where $\Delta k=0$. r is arbitrary and at criticality we can choose it such that all the $\hbar$ dependence appears in a factor in front of ΔI: letting $r=-\ln\hbar/\ln|\alpha\beta|$, then

$$v(\Delta I,\hbar,0)|_{\rm criticality} = \hbar^{\sigma} v(\hbar^{-\sigma}\Delta I, 1, 0), \tag{23}$$

where

$$\sigma = \left(1+\frac{\ln|\alpha|}{\ln|\beta|}\right)^{-1}.$$

This implies that, in the critical case, whatever the transition matrix element may be, $\hbar$ and action appear together as $\Delta I/\hbar^{\sigma}$. This gives the tunneling dependence. We note that this result was also obtained in Ref. [10] where scaling was invoked inside a time integral whose upper limit extended to infinity. Even though scaling does not hold for most of the times in the integral, the result holds up numerically: the exponential dependence of the integral is almost independent of time. Why this is so is still an open question.

Near the subdominant symmetry line, $\sigma\approx 0.65$ whereas near the dominant symmetry line $\sigma\approx 0.76$: the numerically measured value 0.66 is very close to that near the subdominant symmetry line. We suggest that the subdominant symmetry line provides the pertinent scaling exponents for tunneling by the following argument: in the cantoral region the motion follows curves parallel to the cantorus, sampling many angles. The overall quantum tunneling across the curves will then be dominated by the scaling exponents giving the smallest σ; this is at the subdominant symmetry line. In Refs. [10,11], it was suggested that the proximity of the extremal action of the cantorus to the subdominant symmetry line was the reason for the appearance of the subdominant σ as the scaling exponent. However, this region does not distinguish itself from the other angles: we reiterate that the contours near the cantorus closely follow curves parallel to the classical cantorus, as does the classical motion.

To further check the reason for the appearance of the subdominat σ we compared the slopes for entering the cantoral region either side. The relevant extremal actions occur at different values of the angle variable depending on the direction of approach: for example for a whisker cantorus at $I>I_o$, the extremal action from entering at actions below the cantorus is in the range $0\rightarrow 1$ but entering from actions above the cantorus the extremal action is approximately $4\rightarrow 5$. Nonetheless, there was no discernible difference in the slopes in the two cases, and the fit is much better to a 0.66 slope than to a 0.75 slope.

Finally, we comment on the $\hbar$ dependence for retunneling across a cantorus away from criticality. We may say that such cantori which are noncritical but have $\hbar > \Delta W$ are ''classically open but quantum-mechanically closed.'' If we use the same r as in the perturbation theory argument above, $\delta^r \Delta k \rightarrow \hbar^{-\ln \delta / \ln \alpha\beta} \delta k$. Evaluating the exponent and writing in terms of the flux, we get

$$\langle I_m^{\mathrm{ex}} | v | I_n^{\mathrm{ex}} \rangle = \hbar^{\sigma} v[\hbar^{-\sigma} \Delta I, 1, (\Delta W/\hbar)^{1/3}]. \tag{24}$$

So, when $\hbar \gg \Delta W$ we expect the dependence to tend towards that of the critical case $\hbar^{-\sigma} \Delta I$. (When $\hbar$ is not appreciably bigger than ΔW, all the $\hbar$ and ΔI dependence are not all in the same factor on the right-hand side and so we cannot easily determine a general tunneling dependence for this case.) Our numerical results support this (Figs. 15, 13, and 9). This is what we might expect: if $\hbar \gg \Delta W$ (and still smaller than the scaling region), then to the quantum mechanics, the cantorus and its immediate neighborhood do not look that different from criticality.

IV. SUMMARY

The effect cantori have on quantum transport is a key question for understanding the dynamics in generic near-integrable systems. We are not the first to study this: the work of Refs. [11,10] in particular has shed much light on this subject. (We also note that recent experiments [32] have investigated the effect of cantori in quantum mechanics.) We developed this work further and discussed some new effects. Our results are illustrated using the whisker map.

The whisker map is interesting in its own right, since it describes the motion near a separatrix, and separatrices with their chaotic layer are ubiquitous in the phase spaces of generic systems. We showed how a local effective standard map parameter can tell us about the degree of stochasticity in the chaotic layer in the classical map and also about the flux through cantori. The classical dynamics in the chaotic layer is one of fast diffusion deep in the layer, impeded by cantori further out in the layer. Classical transport is slowed at the cantori but eventually trajectories make it through and roam all over the chaotic layer. In contrast, quantum states are exponentially localized throughout the layer, the localization length depending on the action. Quantum transport, even in the long-time limit, is then exponentially suppressed. Deep in the chaotic layer, there is dynamical localization similar to that in the kicked rotor problem at large kick strength. This mechanism is well understood. Much stronger localization happens at cantori further out in the layer. There may be several effective cantori in the layer, increasing in their effectiveness in slowing down transport.

The major results concerned localization mechanisms and $\hbar$ dependences of transport properties at cantori. We pointed out that our results concerning this hold not just for cantori in the whisker map, but rather for any cantori in generic maps due to the universality of behavior near cantori. We found there were two mechanisms resulting in quantum exponential decay at cantori: one, when $\pi\hbar < \Delta W$, is a dynamical localization similar to that in the deep chaotic layer, the other, at $\pi\hbar > \Delta W$ is a retunneling when quantum mechanics sees a closed cantorus, due to the finite $\hbar$ being too big to resolve the gaps. Each mechanism has different characteristics and $\hbar$ dependences than the usual dynamical localization and ordinary tunneling as is described in the text. This is due to the intricate structure of the phase space there and the resulting scaling properties. Which mechanism is at work can be deduced either by looking in the time domain or at a time-averaged probability.

We also argued that the exponential $\hbar$ dependence, discussed at the critical kicked rotor cantorus in the literature, holds for an almost critical cantorus in the whisker map and for noncritical cantori provided $\hbar$ is somewhat bigger than ΔW. We provide numerical evidence as well as an argument based on scaling and perturbation theory to support this. We stress again that these properties should hold for generic cantori.

We considered time-averaged probabilities as well as time development of distributions to demonstrate our numerical results. A final contribution of this paper is a phase-space representation of the quantum mechanics which shows the cantoral regions in the quantum mechanics more clearly than in an action representation. This picture is also useful to bear in mind when considering behavior near cantori and the onset of exponential decay.

ACKNOWLEDGMENTS

N.T.M. would like to thank Lev Kaplan and Steve Tomsovic for very useful discussions and Adam Lupu-Sax and Alex Barnett for help with numerical work. This research was supported by the National Science Foundation under Grant Nos. 66-701-7557-2-30 and CHE9610501.

[1] G.M. Zaslavsky and N.N. Filonenko, Sov. Phys. JETP **38**, 317 (1974); M.V. Berry and M. Tabor, Proc. R. Soc. London, Ser. A **349**, 101 (1976); M. V. Berry in *Les Houches Session XXXVI 1981, Chaotic Behavior of Deterministic Systems*, edited by G. Iooss, R. H. Helleman, and R. Stora (North-Holland, Amsterdam, 1983); M. L. Mehta, *Random Matrices and the Statistical Theory of Energy Levels* (Academic, New York, 1965); *Statistical Theory of Spectra*, edited by C. E. Porter (Academic, New York, 1965).

[2] R.B. Shirts and W.P. Reinhardt, J. Chem. Phys. **77**, 5204 (1982).

[3] S. Tomsovic and E.J. Heller, Phys. Rev. Lett. **70**, 1405 (1993).

[4] E.J. Heller, Phys. Rev. Lett. **53**, 1515 (1984).

[5] R.S. MacKay, J.D. Meiss, and I.C. Percival, Physica D **13**, 55 (1984).

[6] R.S. Mackay, Physica D **7**, 283 (1983; in *Nonlinear Dynamics of Particle Accelerators*, edited by J.M. Jowett, M. Month, and S. Turner, Springer Lecture Notes in Physics No. 247 (Springer, Berlin, 1986) p. 390.

[7] D. Bensimon and L.P. Kadanoff, Physica D **13**, 82 (1984).

[8] S.J. Shenker and L.P. Kadanoff, J. Stat. Phys. **27**, 631 (1982).

[9] D.F. Escande and F. Doveil, J. Stat. Phys. **26**, 257 (1982).

[10] S. Fishman, D.R. Grempel, and R.E. Prange, Phys. Rev. A **36**, 289 (1987).

[11] G. Radons, T. Geisel, and J. Rubner, Adv. Chem. Phys. **73**, 891 (1989); T. Geisel, G. Radons, and J. Rubner, Phys. Rev. Lett. **57**, 2883 (1986).

[12] O. Bohigas, S. Tomsovic, and D. Ullmo, Phys. Rep. **223**, 43 (1993).
[13] R.S. MacKay and J.D. Meiss, Phys. Rev. A **37**, 4702 (1988).
[14] N. Bubner and R. Graham, Phys. Rev. A **43**, 1783 (1991).
[15] G. Györgi, R. Graham, and R.E. Prange, J. Stat. Phys. **68**, 175 (1992).
[16] B.V. Chirikov, Phys. Rep. **52**, 263 (1979).
[17] G.M. Zaslavsky and N.N. Filonenko, Sov. Phys. JETP **27**, 851 (1968).
[18] A.J. Lichtenberg and M.A. Lieberman, *Regular and Chaotic Dynamics*, 2nd ed. (Springer-Verlag, New York, 1992).
[19] I. Percival, *Nonlinear Dynamics and the Beam-Bèam Interaction*, edited by M. Month and J.C. Herrera, AIP Conf. Proc. No 57 (AIP, New York, 1979), p. 302; S. Aubry, in *Solitons and Condensed Matter Physics*, edited by A.R. Bishop and T. Schneider (Springer, Berlin, 1978), p. 264; J.N. Mather, Topology **21**, 457 (1982).
[20] J.M. Greene, J. Math. Phys. **20**, 1183 (1979).
[21] I. Dana and S. Fishman, Physica D **17**, 63 (1985).
[22] J.H. Jensen, and Q. Niu, Phys. Rev. A **42**, 2513 (1990).
[23] N.T. Maitra and E.J. Heller, Phys. Rev. A **61**, 012107 (2000).
[24] D.R. Grempel, R.E. Prange, and S. Fishman, Phys. Rev. A **29**, 1639 (1984).
[25] M. Frigo and S.G. Johnson, URL http://theory.lcs.mit.edu/ fftw (unpublished).
[26] G. Casati, B.V. Chirikov, F.M. Izrailev, and J. Ford, in *Stochastic Behavior in Classical and Quantum Hamiltonian Systems*, Vol. 93 of Lecture Notes in Physics, edited by G. Casati and J. Ford (Springer, Berlin, 1979).
[27] B.V. Chirikov, F.M. Izrailev, and D.L. Shepelyansky, Sov. Sci. Rev., Sect. A **2**, 209 (1981).
[28] Hogg and B.A. Huberman, Phys. Rev. Lett. **48**, 711 (1982).
[29] P.W. Anderson, Phys. Rev. Lett. **109**, 1492 (1958); P.W. Anderson, Rev. Mod. Phys. **50**, 191 (1978).
[30] F. Haake, *Quantum Signatures of Chaos* (Springer-Verlag, Berlin, 1991).
[31] G.O. Morrow and L.E. Reichl, Phys. Rev. E **57**, 5266 (1998); Li Huoming and L.E. Reichl, Phys. Rev. A **42**, 4543 (1990).
[32] B.G. Klappauf, W.H. Oskay, D.A. Steck, and M.G. Raizen, Physica D **131**, 78 (1999); K. Vant, G. Ball, H. Ammann, and N. Christensen, Phys. Rev. E **59**, 2846 (1999).